Chapter 6

Multiterawatt Hybrid (Solid/Gas) Femtosecond Systems in the Visible

Leonid D. Mikheev and Valery F. Losev

Additional information is available at the end of the chapter

http://dx.doi.org/10.5772/63972

Abstract

A novel hybrid (solid/gas) approach to the development of femtosecond high-intensity laser systems operating in the visible is presented in this chapter. Behind this approach is a combination of a solid-state front end relying on widespread and highly developed techniques for femtosecond pulse generation in the near infrared with a photochemically driven boosting amplifier operating in the visible spectral range. Historical background of developing photochemically pumped gas lasers on broad bandwidth electronic transitions in molecules and physical principles of their operation are briefly summarized as well. The architecture and the design issues of the hybrid femtosecond systems relying on the amplification of the second harmonic of Ti:sapphire front ends in the photodissociation XeF(C-A) power-boosting amplifiers driven by the VUV radiation from electron-beam-to-VUV-flash converters are described, as well as breakthrough results of proof-of-principle experiments demonstrating a high potential of the hybrid approach. Wavelength scaling of laser-matter interaction is shortly discussed to demonstrate advantages of shorter driver wavelengths for some applications with main emphasis placed on recombination-pumped soft X-ray lasers.

Keywords: hybrid femtosecond systems, visible spectral range, photochemically driven laser media, laser-matter interaction

1. Introduction

Significant progress in the development of all-solid-state femtosecond laser systems relying on chirped-pulse amplification (CPA) technique has resulted in reaching petawatt (PW) peak powers [1] and focused intensities as high as 10^{22} W/cm^2 [2] that provides great opportunities for experimental studies in the area of the extreme high-field science. The all-solid-state

laser systems providing pulses shorter than 100 fs are based on the Ti:sapphire and optical parametric chirped-pulse amplification (OPCPA) technologies.

Presented in this chapter are milestones and main results obtained in the course of the realization of a novel hybrid (solid/gas) approach to the development of femtosecond systems that, unlike the all-solid-state systems operating in the near-infrared (NIR) region, allow for producing super-intense optical pulses in the blue-green spectral range. This approach aims to marry robust solid-state laser technologies highly developed for femtosecond pulse generation and amplification in the NIR spectral range with advantages of photochemically driven gaseous gain media of the visible range.

Most extensive development of the photochemical method of pumping gaseous active media dates back to the 1960s–1990s of the last century (see [3–5] and references cited therein). Being applied to optical excitation of gas lasers on electronic molecular transitions by radiation from such unconventional pump sources as high-temperature electrical discharges and strong shock waves in gas, This method resulted in emerging a new class of gaseous active media for lasers emitting in the spectral range extending from the NIR to UV with a high output energy increasing in proportion to the active volume and pump energy. Among a variety of molecules lasing upon optical excitation, there are three broadband active media (XeF(C-A), Kr_2F, and Xe_2Cl), which offer a number of characteristics extremely attractive for the amplification of femtosecond optical pulses up to ultrahigh peak powers. The gaseous nature and visible spectrum of emission of these media promise important virtues of the hybrid systems. First of all, the gaseous nature of these media is characterized by low nonlinear refractive index allowing amplification of optical pulses with much higher intensities as compared with solid media. Secondly, the visible spectrum of emission requires nonlinear frequency upconversion of a seed pulse generated in the NIR spectral region by a solid-state front end, thereby providing efficient temporal cleaning of the ultrashort optical pulse and the high temporal contrast ratio of an output pulse, which is of primary importance for a number of high-field experiments.

The main motivation for the development of hybrid systems in the visible is favorable drive frequency scaling of laser-matter interaction in a number of high-field applications. Of overriding importance is the dramatic improvement of the recombination soft X-ray laser excitation in an optical field ionized (OFI) plasma with drive frequency.

2. Photochemical lasers

The photochemical method of gaseous active media pumping by radiation from broadband optical sources originates from the development of the high-power photodissociation laser in metastable iodine atoms ($\lambda = 1.315$ μm) (for example, see [6–8]), resulted in variety of remarkable results: 1 MJ of output energy in a single beam [9], 2 and 30 kJ in a short laser pulse obtained, respectively, with flash lamp [10] and surface discharge [11] optical pumping. The breakthrough results obtained in the course of the iodine photodissociation laser development stimulated extensive studies of the potentialities of the gaseous active media optical

http://dx.doi.org/10.5772/63972

pumping and the search for new active media for high-power optically driven lasers in many laboratories around the world.

It is important to stress the major impact of untraditional pumping sources on the photochemical method development, such as high-current open discharges initiated with exploding wires or sliding sparks, as well as strong shock waves driven by detonation of chemical explosives [4]. These pumping sources, initiated directly in laser working mixtures, had no shell separating them from an active medium that removes limitations on energy deposition into the pumping sources and makes it possible to utilize the radiation in any spectral range, including the UV and VUV, where the most intense absorption bands of the overwhelming majority of molecules are located. As compared with ordinary flash lamps, these pumping sources have much higher brightness temperature reaching 30–35 kK.

The main emphasis in these studies was placed on molecular transitions that, unlike atoms, do not require complete population inversion of the electronic states participating in the laser transition and enable a fairly simple depletion of the lower laser levels due to vibrational relaxation and/or dissociation of the lower state. The application of such optical sources has led to emerging new class of gas lasers emitting in the spectral range from the NIR to UV regions due to the development of a variety of photochemical excitation techniques relying on the photolysis and direct optical excitation of molecular gases, as well as secondary photochemical reactions (see [3–5] and references cited therein).

One of the most remarkable results obtained in the course of these studies is the optical excitation of lasing on broadband bound-free $Kr_2F(4\ ^2\Gamma\text{-}1,2\ ^2\Gamma)$, $Xe_2Cl(4\ ^2\Gamma\text{-}1,2\ ^2\Gamma)$, and XeF(C-A) transitions in the visible. These active media are very sensitive to the internal losses because they have much lower small-signal gain as compared with excimers emitting in the UV spectral range on the B-X transition due to the large width of their luminescence spectra and long radiative lifetime of the excited states. For this reason, e-beam or fast discharge pumping of these active media turned out to be ineffective since electron excitation technique is based on plasmochemical reactions involving ionized and highly excited atoms and molecules that are characterized by strong absorption in the visible [12]. For example, laser action from electron-beam-excited Kr_2F and Xe_2Cl active media was observed only in the afterglow of the pump pulse when the transient absorption is significantly reduced [13]. The photochemical technique, relying on reactions of neutrals excited to low-lying energetic states, free of the shortcomings associated with transient absorption. This makes optical pumping to be superior to electron excitation in the efficiency of producing laser action on the aforementioned transitions.

Due to extremely broad gain bandwidth supporting pulses of shorter than 10 fs, these active media are of practical interest for amplifying femtosecond optical pulses to ultrahigh peak powers [4, 5, 14, 15]. The main spectroscopic characteristics of the transitions are listed in the **Table 1**. One of most important parameters is the saturation fluence accounting for the maximum energy extraction per surface unit of an amplifier output aperture. This parameter, ranging from 0.05 J/cm^2 for XeF(C-A) to 0.2 J/cm^2 for Kr_2F due to rather long radiative lifetime of the upper laser states, promises peak power, I_{out}, of up to ~10 TW per square cm of an output aperture in a 25 fs pulse. At the same time, the gas active media are easily scalable to large volumes with wide aperture (several hundred cm^2) to reach PW level of output peak

power. Moreover, the combined use of two media with spectrally shifted emission bands (Kr_2F with XeF(C-A) or Xe_2Cl) in an amplifier chain makes promising for the amplification of even shorter optical pulses due to twofold broadening a gain bandwidth (**Figure 1**) and spectrally inhomogeneous gain saturation.

Transition	**XeF(C-A)**	**$Kr_2F(4^2\Gamma\text{-}1,2^2\Gamma)$**	**$Xe_2Cl(4^2\Gamma\text{-}1,2^2\Gamma)$**
λ_{max}, nm	480	420	510
$\Delta\lambda$, nm	70	80	100
τ_{FT}, fs	5	3	4
τ_{sp}, ns	100	180	250
σ_{st}, cm^2	10^{-17}	2.3×10^{-18}	2.8×10^{-18}
ε_{sat}, J/cm^2	0.05	0.2	0.15
I_{out} ($\tau = 25$ fs), TW/cm^2	2	8	6

λ_{max} is the wavelength of the gain maximum.
$\Delta\lambda$ is the gain bandwidth.
τ_{FT} is the transform-limited pulse width (for Gaussian profile).
τ_{sp} is the spontaneous lifetime.
σ_{st} is the stimulated emission cross-section.
ε_{sat} is the saturation fluence.
I_{out} is the estimated maximum peak power density related to a laser amplifier output aperture.

Table 1. Characteristics of broadband active media.

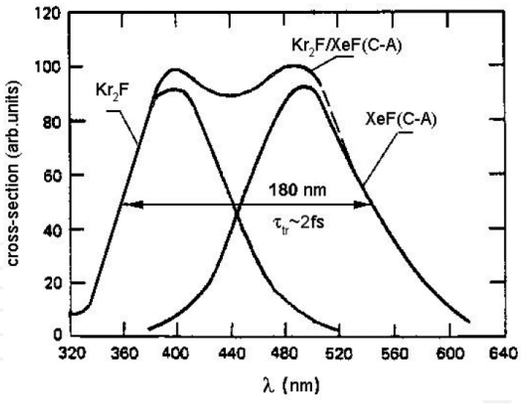

Figure 1. Emission spectrum for the mixed Kr_2F/XeF(C-A) system.

An important advantage of gaseous active media resides in the much lower value of the nonlinear index of refraction as compared with solid-state materials, which allows amplification of optical pulses at much higher intensities than in condensed gain media. For the first time, hybrid architecture employing a gaseous active medium was realized in the system comprising a dye femtosecond oscillator and e-beam or fast discharge-driven boost amplifier on the UV B-X transitions of ArF, XeCl, KrF, and XeF rare-gas-halide excimer molecules.

http://dx.doi.org/10.5772/63972

The highest peak power obtained in the hybrid systems of this type reached ~1 TW in a 310 fs pulse [16]. However, gain bandwidth on the B-X transition does not exceed 2 nm in full width at half-maximum (FWHM) corresponding to the spectrally limited pulse width of ~50 fs. With spectral gain narrowing in amplifiers, it is difficult to count on the possibility of producing pulses shorter than 0.1 ps at the TW level of peak power. Moreover, due to the short spontaneous lifetime of the B state and rather narrow spectral bandwidth, these transitions exhibit as low as 1 mJ/cm^2 saturation fluence, which corresponds to the output intensity of 10^{-2} TW/cm^2 in a 0.1 ps pulse, requiring too large output aperture to produce multiterawatt output peak power.

Compared with the B-X transition, the broadband photochemical media are characterized by more than an order of magnitude larger gain bandwidth and saturation fluence allowing for several TW/cm^2 to be obtained in hybrid systems comprising these active media. In addition, unlike to the electron-impact excitation, the optical pumping, which is practically free of transient absorption within the laser transition spectral band, makes the entire transition bandwidth to be accessible for the femtosecond pulse amplification. These active media are briefly reviewed in the subsequent sections.

2.1. XeF(C-A) active medium

A schematic energy diagram of the upper and lower XeF laser levels is shown in **Figure 2**. Behind the optical pumping XeF active medium is the photolysis of XeF_2 vapor in the spectral range of <204 nm to produce XeF excimers mainly in the B state [17–19]. The C state, lying lower than the B state, is populated due to collisional relaxation of the latter in the presence of a buffer gas. Depending on composition of working mixture, laser action is observed on the B-X (353 nm) or C-A (480 nm) transition [20]. Broad gain bandwidth on the C-A transition ($\Delta\lambda = 70$ nm [21]) is accounted for by the repulsive nature of the A state. On the other hand, repulsive character of the lower A state provides its virtually instantaneous depopulation and ensures population inversion independently on the presence of buffer gas.

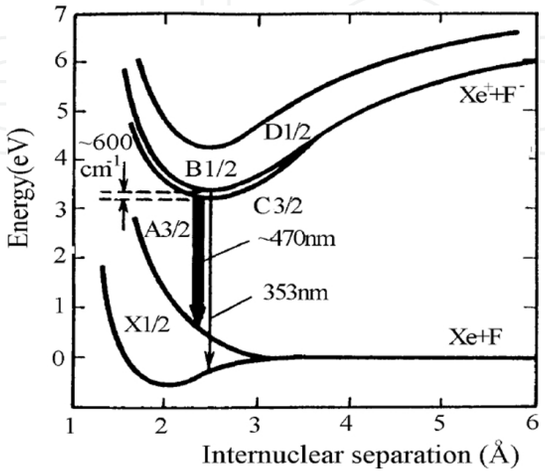

Figure 2. The potential curves of low-lying energetic states of the XeF excimer molecule.

Lasing in the photochemically driven XeF active medium was obtained for the first time in 1977 on the *B-X* transition with an exploding wire as a pump source [22]. Later on, in a series of papers, laser action on XeF(B-X) and XeF(C-A) was reported upon optical pumping by broadband VUV radiation from exploding wires [20, 23], surface discharges [24–27], formed-ferrite flash [28, 29], and strong shock waves [30], as well as by the Xe_2 spontaneous emission at 172 nm excited by an electron beam [31–33]. These studies have led to a number of significant achievements. Among them are high output energies attaining as much as 1 kJ and 170 J in the UV region with the strong shock wave [30] and surface discharge optical pumping [24], respectively, as well as 120 J and 10 J obtained in the visible under optical pumping by radiation from surface discharges operating in the single shot [24] and 1 Hz repetitive rate [27] modes respectively.

Studies of the XeF(C-A) laser showed that, besides minor transient absorption discussed above, the optical pumping XeF(C-A) active medium has an additional advantage over the electron-impact excitation, which consists in the much weaker competition of the B-X transition. The point is that upon optical excitation, relative populations of the closely lying B and C states are determined by the thermodynamic equilibrium at a buffer-gas temperature that is close to the room temperature, while, upon e-beam and fast discharge pumping, the main role in the energy exchange between these states is played by secondary electrons, which have a temperature of ~1 eV characteristic of this pumping. In the optically driven active medium, the electron concentration is negligibly low, thereby providing an efficient laser action on the C-A transition.

From the viewpoint of femtosecond pulse amplification, the pump technique relying on the e-beam-driven spontaneous emission of Xe_2 excimers is of particular concern because, along with surface discharge optical pumping, it paved a new way for the development of the hybrid (solid/gas) femtosecond systems in the blue-green region. With the use of this technique to pump the XeF(C-A) laser, as high as 6 J of output energy was reported in [33].

Finally, it is essential to note that one of the most important conclusions gained from the optically driven XeF(C-A) laser studies is that at a proper composition of the active medium its broad amplification band is not practically modified by transient absorption making the entire transition bandwidth to be accessible for the femtosecond pulse amplification. A drawback of the XeF(C-A) active medium is that it must be replaced in a laser chamber after each shot because of the photodecomposition of the parent XeF_2 molecules.

2.2. Xe_2Cl active medium

Among the broad bandwidth photochemically driven active media listed in **Table 1**, Xe_2Cl is of special interest because initial working mixture is not consumed throughout pump flash allowing for operation in the repetitive mode without replacing the working gas mixture after each shot. Moreover, as compared with the XeF(C-A) transition, this active medium has a much longer radiative lifetime of the upper state, which was measured to be 245 ns [34].

This active medium, as well as Kr_2F discussed below, is currently studied to a much lesser extent as compared with XeF. First observation of lasing in the Xe_2Cl triatomic excimer was

http://dx.doi.org/10.5772/63972

reported in 1980 upon e-beam pumping [35]. This was followed in 1985 by successful operation of the Xe_2Cl laser optically pumped by the VUV radiation at 137 nm from the open discharge initiated by an exploding wire [36]. Behind the laser action is the reaction of optically excited molecular chlorine with Xe to form XeCl(B) excimers that then recombine with xenon into Xe_2Cl^* emitting in the blue-green region with a fluorescence quantum yield experimentally measured to be ~75%, with respect to the absorbed pumping photons [37].

However, the application of this technique for the femtosecond pulse amplification is of little practical significance since, due to the narrow Cl_2 absorption bandwidth at 137 nm, an efficiency of the Xe_2Cl pumping by the thermal pump source is expected to be low. Moreover, to take advantage of repetitive pulse mode of operation, it requires the development of a powerful large-area pumping source radiating in the short-wave part of the VUV spectral range in a repetitive pulse regime.

On the other hand, as was shown in [38], more promising is the excitation of the active medium in mixtures of Xe and $C1_2$ vapor due to the photoassociation process

$$Xe + Cl + hv \rightarrow XeCl(B,C)$$

at the wavelength of a XeCl laser (308 nm) followed by the three-body XeCl(B,C) recombination with xenon to form $Xe_2Cl(4\ ^2\Gamma)$. Production of Cl atoms is provided by the same pump pulse of the XeCl laser via photodissociation of $C1_2$. In the mixtures of Xe and Cl_2 at pressures of 1–2 bar and 1–2 Torr, respectively, the quantum efficiency for the energy transfer from XeCl(B,C) to $Xe_2Cl(4\ ^2\Gamma)$ is close to 100% due to the extremely high rate constant (1.3×10^{-30} cm^6 s^{-1} [39]) of the XeCl(B,C) recombination with xenon. The main loss process in the pump mechanism considered here is the $C1_2$ photodissociation to accumulate a sufficient number of Cl atoms and thereby ensure a high enough absorption of pump photons in the longitudinal geometry of excitation. Nevertheless, the overall efficiency for the conversion of the pump energy into the energy stored in the Xe_2Cl active medium is estimated to be as high as 5% at the pump intensity of 5 MW/cm^2 in a 100 ns pump pulse. According to Ref. [38], this mechanism of pumping can be of great practical importance, since it enables to produce a small-signal gain in the Xe_2Cl active medium, which is expected to be even higher than that obtained in the XeF(C-A) amplifier to be discussed later. Moreover, molecular chlorine is not consumed upon optical excitation because chlorine atoms, generated in the Cl_2 photodissociation, recombine back to the molecular state at a time scale of 1 ms. This makes it far easier to operate a Xe_2Cl femtosecond amplifier in the pulse repetition regime.

For the sake of completeness, it should be noted that the gain on the Xe_2Cl laser transition excited due to photoassociation at 308 nm was observed for the first time in chlorine-doped solid [40] and liquid [41] xenon. However, unlike gaseous active media, realization of the femtosecond pulse amplifier based on this technique is a serious technological problem.

2.3. Kr_2F active medium

Emission band of Kr_2F at 420 nm is spectrally shifted relative to emissions of XeF(C-A) at 480 nm and Xe_2Cl at 490 nm that enables twofold broadening of the amplification band (**Figure 1**) with the use of two different active media in an amplifier chain.

The Kr_2F excitation mechanism relies on the KrF_2 photodissociation absorption in the VUV spectral range around 164 nm [42] to produce KrF(B) excimers. The utilization of KrF(B) in secondary processes is different, depending on the composition and pressure of the working mixture. For example, in low-concentration Xe admixtures, exchange processes take place, resulting in XeF(B) formation with a yield close to 100% and laser action at 353 nm upon pumping by radiation from exploding wire [42]. Being mixed with Kr at a pressure of ~1 bar, KrF(B) forms $Kr_2F(4\ ^2\Gamma)$ excimers in three-body recombination collisions [43].

It was found that the laser action in Kr_2F^* also occurs if, instead of Kr, nitrogen is admixed to the working mixture. This observation was attributed to the formation of KrN_2F^* four-atomic excimers that produce Kr_2F^* in exchange reactions with Kr atoms generated upon photochemical decomposition of KrF_2 vapor by VUV pump radiation [43]. Note that, despite a complex Kr_2F^* formation mechanism, which involves three stages of chemical transformations in mixtures with nitrogen (at one of the stages, products of photochemical processes react with each other), the Kr_2F^* yield is rather high providing ~70% of KrF(B) molecules to be transformed into Kr_2F^* excimers [43]. Lasing in Kr_2F at 450 nm was observed upon optical pumping of KrF_2:N_2 = 1:1500 Torr and KrF_2:CF_4:Kr = 1:300:1200 Torr gas mixtures by the VUV radiation from an open discharge initiated by an exploding wire [44].

The most detailed results of experimental investigations of above considered broadband active media and a complete bibliography on the works can be found in Refs. [3, 20, 45].

3. Hybrid systems with XeF(C-A) amplifiers

Among the gaseous active media with broad amplification band, XeF(C-A) is the most widely studied. That is why this transition was the first to study the hybrid approach with the use of the broadband excimer molecules. Studies of the femtosecond pulse amplification on the XeF(C-A) transition were pioneered by demonstration of 1 TW peak power due to the direct amplification of 250 fs seed pulses from a mode-locked dye laser in the e-beam-driven active medium [15]. However, application of electron-beam excitation to the XeF(C-A) active medium faces serious difficulties associated with the above mentioned transient absorption and competition of B-X and C-A transitions due to strong mixing of closely lying *B* and *C* states of the XeF excimer by electrons. As it was discussed above, transient absorption results in the afterglow gain formation. Strong B-C states mixing causes C-state depopulation via ASE depletion of the B-state which has two orders of magnitude higher stimulated emission cross section for the B-X transition compared with that for the C-A transition. Using five-component mixture comprising F_2, NF_3, Xe, Kr, and Ar has circumvented this problem due to formation of Kr_2F excimers strongly absorbing emission at the wavelength of the B-X transi-

tion (353 nm). As discussed above, optical pumping of this active media is free of both of these shortcomings.

3.1. Hybrid systems based on surface discharge-driven XeF(C–A) amplifiers

Beginning with the proposal of femtosecond pulse amplification in the optically driven XeF(C-A) active medium [14], experimental studies in the field of the hybrid (solid/gas) technology started with the development of the XeF(C-A) amplifier optically driven by the VUV radiation from large-area multichannel surface discharges (see [5] and references cited therein). For this purpose, two versions of the photochemically driven XeF(C-A) amplifier based on the surface discharge as an optical pump source have been built at the P.N. Lebedev Physical Institute (LPI, Moscow, Russia) and at the Lasers Plasmas and Photonic Processes (LP3) Laboratory (Marseille, France) (**Figure 3**). They differ from each other by an output aperture (3×11 and $5 \times 18\ cm^2$, respectively), discharge initiation technique, and pump energy. Pumping sources are based on the multichannel surface discharges initiated along the side walls of rectangular half a meter long dielectric chambers filled with a mixture of XeF_2 vapor, argon, and nitrogen at 1 atm. The pumping scheme, in which two planar sources pump an active medium placed between them, provides spatially homogenous excitation of the medium. Moreover, rectangular aperture of the designed amplifiers offers a simple approach to the development of the multipass optical scheme for energy extraction from XeF(C-A) active medium characterized by rather low values of small-signal gain upon optical pumping. In a multipass scheme of the "wedge-trap configuration," a seed pulse runs between two tilted intracell mirrors allowing for up to 45 double passes through the active medium to be realized.

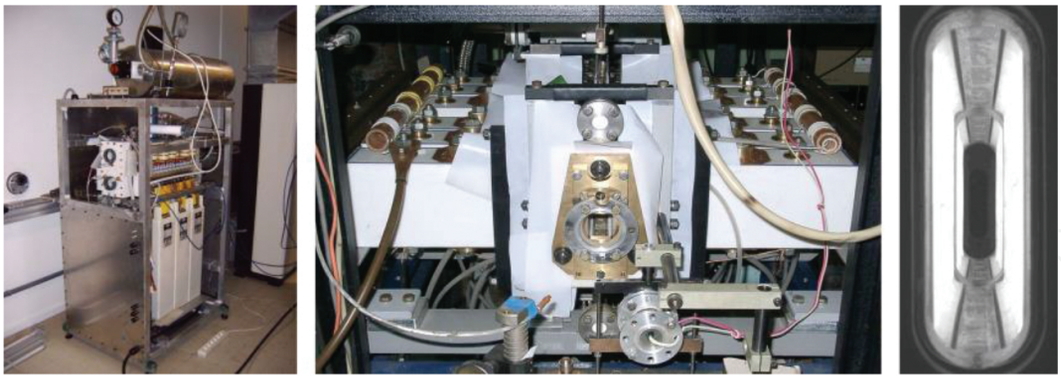

a b c

Figure 3. Photographs of the XeF(C-A) amplifiers built at (a) LP3 and (b) LPI. (c) Inside view of the amplifier cell with multichannel surface discharges fired along its side walls.

Operating performances of the XeF(C–A) amplifier, which were measured at the LP3 Laboratory with the use of a hybrid Ti:sapphire/optical-parametric-amplifier front end system, demonstrated a total multipass gain factor of 10^2, corresponding to a small-signal gain of $2 \times 10^{-3}\ cm^{-1}$, with spectrally and spatially homogeneous amplification.

More details and a complete bibliography on the operating characteristics of the laser amplifier and pump sources relying on the multichannel surface discharge are summarized in [5].

3.2. Hybrid systems based on XeF(C-A) amplifiers pumped by the VUV radiation of e-beam converter

The promising results obtained in the course of the studies of the surface discharge pumped XeF(C-A) amplifiers motivated the development of an alternative pump technique based on the conversion of e-beam energy to the VUV radiation, which is expected to be more practical from the viewpoint of the XeF(C-A) amplifier scaling. The main principle of laser action upon pumping by the e-beam excited xenon emission was introduced for the first time in [31] to pump a XeF(B-X) laser operating in the UV region. Later on, this technique was applied to pump a multijoule XeF(C-A) laser in the visible [33].

To study this approach, two hybrid fs systems, THL-30 with a design peak power of ~10 TW and THL-100 designed for 50–100 TW peak power, have been built at the LPI and Institute of High-Current Electronics (IHCE, Tomsk, Russia), respectively. Both of these systems comprise Ti:sapphire front ends (Avesta Project Ltd), frequency doublers, prism pair stretcher, and power-boosting XeF(C-A) amplifiers driven by e-beam-to-VUV-flash converters made at the IHCE.

3.2.1. THL-30 hybrid system

Photos of the front end and XeF(C-A) amplifier incorporated into the THL-30 hybrid system are presented in **Figure 4**. **Figure 5** shows the cross sectional schematic diagram of the XeF(C-A) amplifier. The e-beam converter (2) of cylindrical form is filled with pure xenon at a pressure of 3 bars. Emission of Xe_2^* is excited by four 120 cm long × 15 cm wide radially converging beams of electrons accelerated up to 450 keV in the vacuum diode (1) and injected into the converter through 40 μm Ti foils. The laser cell (3) consists of a 12 × 12 × 128 cm square cross-sectional tube with arrays of 10 rectangular CaF_2 windows (12 × 12 cm) sealed on its side walls. The cell containing XeF_2/N_2 mixture at 0.25–1 bar is housed into the e-beam converter along its axis. In this configuration, the laser cell is thus immersed into the xenon. The distance of 7.5 cm between the Ti foil and CaF_2 windows is chosen to assure that the electrons issued from the e-beams are stopped in the converter at the xenon operating pressure of 3 bars. The e-beams excite the xenon over a 250 ns pulse to produce Xe_2^* fluorescence at 172 nm with a ~30% average fluorescence efficiency [33]. The Xe_2^* radiation is transmitted through arrays of CaF_2 windows into the laser cell to photodissociate XeF_2. The e-beam energy deposited into xenon is measured to be 2.5–3 kJ, which yields a small signal gain of (1.5–2.5) × 10^{-3} cm^{-1} in the laser cell [46, 47].

http://dx.doi.org/10.5772/63972

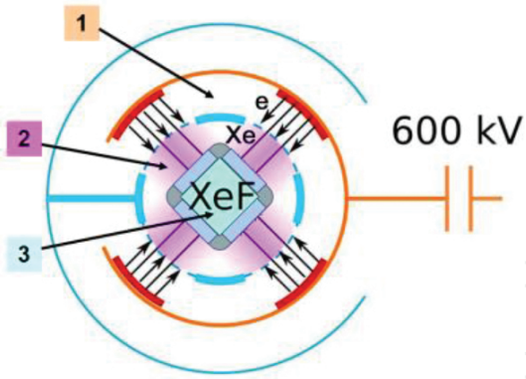

Figure 5. Cross-sectional schematic diagram of the XeF(C-A) amplifier: (1) vacuum diode, (2) e-beam converter, and (3) photolytic laser cell.

Seed pulses with 50 fs duration and 5 mJ energy at 475 nm are produced in the solid-state front end consisting of a Ti:sapphire oscillator operating at 950 nm, regenerative and multipass amplifiers, and KDP frequency doubler spectrally matching the front end to the boosting XeF(C-A) amplifier. Nonlinear frequency upconversion also allows for temporal cleaning of seed pulses injected into the final gas amplifier.

Before the final amplification, the seed pulses are negatively chirped to 1 ps with the use of a prism-pair arrangement. Besides avoiding nonlinear pulse distortion in the amplifier, seed pulse stretching is required to exceed the rotational reorientation time of the XeF(C) molecules, which is estimated to be about 0.8 ps [48, 49]. If the seed pulse is linearly polarized and shorter than the above value, saturation of only a portion of all excited XeF molecules is possible (because of random molecular orientation), thus limiting energy extraction from the amplifier. Down-chirped pulses can be then recompressed due to the positive group velocity dispersion in bulk glass and/or chirped mirrors.

A multipass optical scheme for energy extraction from the active medium has a 3D "wedge-trap" configuration formed by two pairs of tilted intracell mirrors providing the displacement of a beam in two mutually orthogonal directions.

In test experiments, an output energy of 0.25 J has been extracted from the amplifier seeded with a 4 mJ pulse [46, 47], indicating that 5 TW peak power can be obtained in THL-30.

Figure 4. THL-30: Photographs of the Ti:sapphire front end (left) and XeF(C-A) amplifier (right).

Presently, this system is mainly used for the development of key technologies purposed for the implementation in the THL-100 system to be discussed below in more detail.

3.2.2. THL-100 hybrid system

Architecture of THL-100 laser is substantially similar to that described above for the THL-30 hybrid system. Its optical scheme is shown in **Figure 6**.

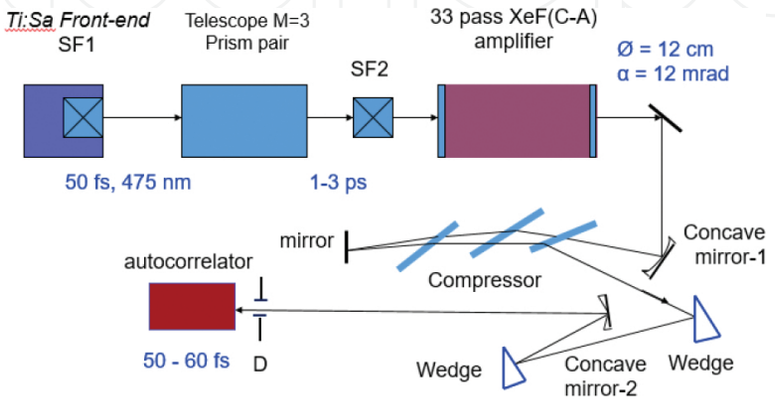

Figure 6. Optical scheme of THL-100 laser system. Ti:Sa front end—Start-480M; SF1 and SF2—vacuum spatial filters; compressor—4-cm-thick fused silica plates at Brewster angle; D—260 μm diaphragm; concave mirror-1—F = 7.5 m; concave mirror-2—F = 12 m.

3.2.2.1. Front end

The front end (Start-480M manufactured by "Avesta Project Ltd") shown in **Figure 7a** consists of a Ti:sapphire master oscillator pumped by a CW pump laser (Verdy-8) at a wavelength of 532 nm, grating stretcher, regenerative and two multipass amplifiers pumped by repetitively pulsed lasers (SOLAR Laser Systems) at a wavelength of 532 nm, spatial filter after the final amplifier, grating compressor, and generator of the second harmonic. The output energy of 20 mJ is produced in a 50 fs pulse at the wavelength of the second harmonic (~475 nm) [50]. The front end operates in the single pulse mode and with a repetition rate of 10 Hz. The output beam of 2.5 cm diameter is directed to the prism pair arrangement (**Figure 7b**) with negative group velocity dispersion, which allows a seed pulse to be stretched. It consists of a mirror telescope with a magnification M = 3, two fused silica prisms allowing a 75-mm-diameter beam to pass, and the mirrors for beam transportation between the prisms in the forward and backward directions. The maximum distance that can be realized between the prisms is 9.6 m, corresponding to the 2.4 ps pulse duration. After the prism pair, the laser beam is directed into the XeF(C-A) amplifier.

Figure 7. (a) Femtosecond Ti:sapphire front end. (b) Prism pair arrangement.

3.2.2.2. Photodissociation XeF(C-A) amplifier

Figure 8 shows a photograph of the XeF(C-A) amplifier. Its principle of operation and the design is similar to the above described XeF(C-A) amplifier of THL-30 laser system. However, it has its differences: the e-beam converter is driven by six electron beams instead of four and its pump energy is four times higher. The amplifier includes two high-voltage pulse generators operating at $U_0 = 90$ kV or 95 kV charging voltage, a vacuum electron diode, gas chamber with a foil support structure, which filled with xenon, and laser cell with two mirror units for multipass amplification of the laser beam. The design and specifications of the XeF(C-A) amplifier are described in detail in [47, 51–54].

Figure 8. General view of the XeF(C-A) amplifier.

An electron accelerator generates six 100 cm long × 15 cm wide electron beams with a maximum energy of 550 keV (at $U_0 = 95$ kV) at the total diode current of 250 kA in a 150 ns (FWHM) pulse. Bunches are injected into the chamber filled with xenon at a pressure of 3 bar. The electron beam energy is converted to the VUV radiation of Xe_2^* excimers at a wavelength of 172 nm with an efficiency of 30–40%. Inside the gas chamber along its axis is the hexagon laser cell (**Figure 9a**), on the side faces of which there are a total of 54 windows made of CaF_2. The

windows with size of 12 × 12 cm and 2 cm thick are set in grooves on the rubber gasket (Viton) and sealed by means of clamping flanges. The windows are arranged opposite grates with foil, through which the electron beam is injected into the gas chamber. This provides the best geometric coupling of the cell with laser pump source. The output aperture of the laser cell has a diameter of 24 cm. Both ends of the laser cell are sealed with fused silica windows with a diameter of 30 cm. Inside the cell, there are two mirror units that provide multiple passage of the seed pulse through the active region. Each unit has 16 mirrors of different diameters arranged along its perimeter. The mirror reflection coefficient is 99.5–99.7%. The laser cell is filled with a gas mixture consisting of 0.25–0.5 bar high purity nitrogen and 0.1–0.4 Torr XeF_2 vapor. **Figure 9b** shows an internal view of the laser chamber with the mirror unit at the rear end. To maximize the efficiency of conversion of the electron beam energy into the VUV radiation, the high purity (99.9997%) xenon is used and the e-beam converter gas chamber is evacuated to a pressure of 10^{-4} Torr. As xenon purity decreases due to exposure of the electron beams to the structural elements of gas chamber, its purification is carried out by a filtering device "Sircal MP-2000."

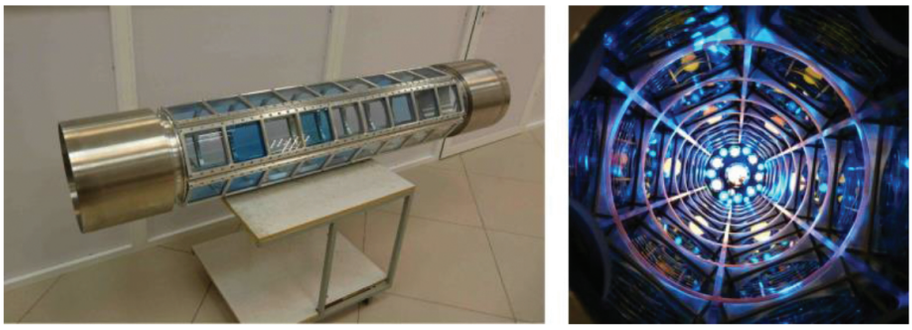

Figure 9. (a) Laser cell of the XeF(C-A) amplifier. (b) Inside view of the laser cell with the mirror unit.

3.2.2.3. Experimental techniques

The active medium of the XeF(C-A) amplifier is created under the action of the VUV radiation at a wavelength of 172 nm. XeF excimer molecules are formed in the B-state via XeF_2 photodissociation. The upper state of the XeF(C-A) laser transition is formed as a result of the relaxation of the XeF(B) molecules in collisions with the molecules of the N_2 buffer gas. Amplification of the seed pulses was carried out in a multipass optical scheme (33 passes). The laser beam entering into the XeF(C-A) amplifier was made slightly divergent, so that during amplification, it was steadily increased in diameter from 20 mm (inlet) to 62 mm (the penultimate mirror), making a double round-trip along the inside perimeter of the laser cell. The penultimate convex mirror directed the beam to a flat mirror 100 mm in diameter, located on the optical axis. After reflection from this mirror, the beam propagated along the optical axis of the cell reaching 120 mm in diameter at the amplifier output.

Small-signal gain distribution over the laser chamber cross section was measured at four passes through the active medium of the XeF(C-A) amplifier with the help of the Sapphire-488 CW semiconductor laser (488 nm). In addition, the total small-signal gain, G, was measured in

the 33 pass amplification scheme. For measuring the power of amplified spontaneous emission (ASE) of the XeF(C-A) amplifier, the output radiation without a seed pulse was focused by concave mirror with a focal length of 22 m on an aperture with diameter 1.1 mm, behind which a filter and calibrated photodiode were located.

Seed pulses of 50 fs duration from the front end were pre-lengthened to 1–2.4 ps in the prism pair with negative group velocity dispersion. After amplification, the down-chirped laser pulses were recompressed in a double pass of a collimated beam with a diameter of 20 cm through three 4-cm-thick fused silica plates at the Brewster angle. Energy losses in the compressor did not exceed 2%. To measure the pulse duration, the central part of the beam (with the help of two fused silica wedges and a spherical mirror with diameter of 90 mm and focal length of 12 m) was assigned to the autocorrelator ASF-20–480 through an aperture with a diameter of 260 μm.

3.2.2.4. Experimental results

The gain characteristics of the active medium (viz. value and spatial distribution of the small-signal gain) depending on the initial composition of the working mixture were examined using 4-passes amplification of the probe laser. The optimal composition of the gas mixture (0.25 Torr XeF_2 and 190 Torr nitrogen) corresponding to the maximum value of the unsaturated total gain ($G = (5–6) \times 10^3$) was found as a result of a compromise between the uniformity of the radial distribution of the small-signal gain and its maximum lying in the peripheral region of the laser cell, where the main part of the beam trajectories is located. It should be noted that the heterogeneity of the small-signal gain distribution over the chamber cross section had almost no effect on the uniformity of the beam intensity, as the diameters of the laser beam and laser cell differ by almost an order of magnitude.

In the test mode, when the maximal pump energy (at $U_0 = 95$ kV) of the VUV radiation was 240 J, the energy of output radiation attained 1 J at amplification of a 1 ps seed pulse with an energy of 1.8 mJ. At the level of 0.7 J output energy, the pulse duration after the bulk fused silica compressor was measured with and without activation of the XeF(C-A) amplifier. In both cases, the pulse width was measured to lie in the range of 50–60 fs (**Figure 10a**). This indicates that a peak power of 14 TW was reached at the output of the laser system [47].

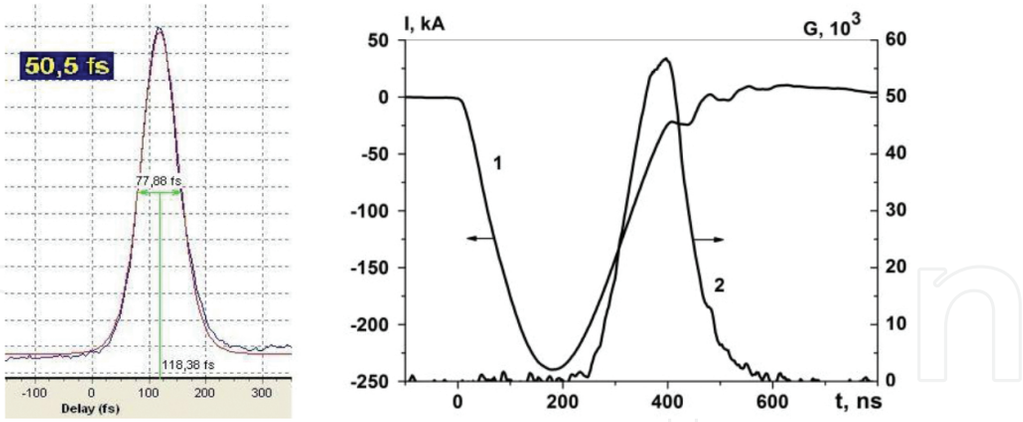

Figure 10. (a) Autocorrelation function of the output pulse with an energy of 0.7 J (in the $Sech^2$ approximation). (b) The time behavior of the diode current (1) and total gain (2). $U_0 = 95$ kV.

The ASE power from the XeF(C-A) amplifier, which was measured in the angle of 0.5 mrad with the seed pulse blocked, turned out to be as low as 0.7 W. At the 14 TW peak power obtained in the above experiments, this ASE power corresponds to the temporal contrast ratio of 2×10^{13}. Since the temporal contrast at the 10^{10} level is now routine to obtain in Ti:sapphire systems, and taking into account the nonlinear frequency doubling required to spectrally match the Ti:sapphire front end to the XeF(C-A) boosting amplifier, the temporal contrast of the hybrid (solid/gas) systems seems to be determined only by the ASE of the XeF(C-A) amplifier and is expected to reach 10^{12}–10^{13} at a peak power of about 100 TW.

For further improvements of the THL-100 operating performances, the XeF(C-A) amplifier pump system has been upgraded [51, 52] to increase the maximum VUV pump energy up to 300 J at $U_0 = 95$ kV. As a result, the total small-signal gain at 33 passes was enhanced up to $(5–6) \times 10^4$. **Figure 10b** shows the temporal behavior of the diode current (1) and total small-signal gain (2) at 33 passes through the active medium. **Figure 11** shows the dependence of the small-signal gain in arbitrary units vs the partial pressures of nitrogen and XeF_2 vapor.

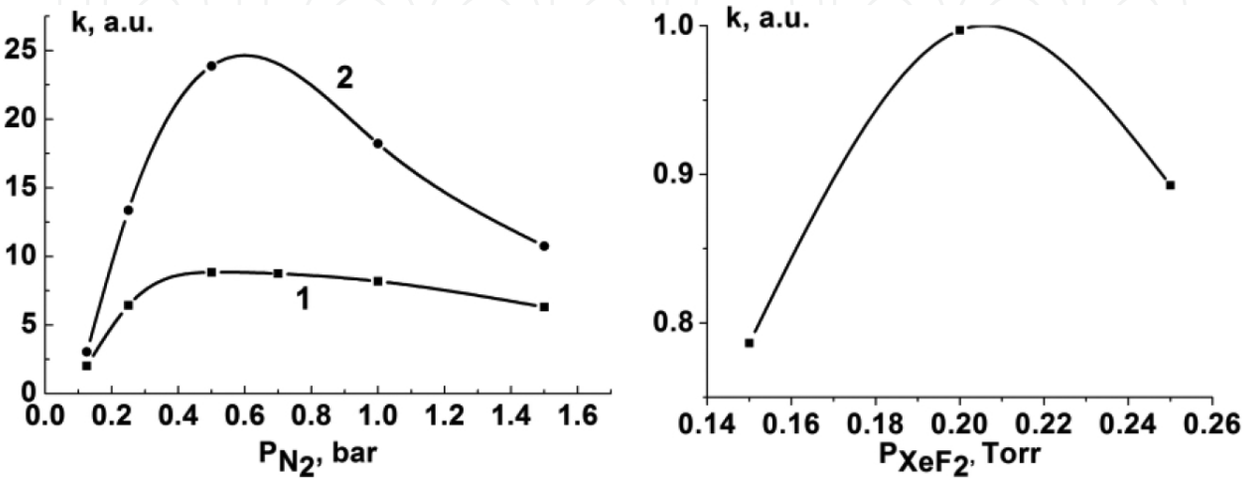

http://dx.doi.org/10.5772/63972

Figure 11. (a) Dependence of the small-signal gain vs the nitrogen pressure, $p(XeF_2) = 0.25$ Torr, $1 — U_0 = 90$ kV, $2 — U_0 = 95$ kV. (b) Dependence of the small-signal gain vs the XeF_2 pressure, $p(N_2) = 0.5$ bar, $U_0 = 90$ kV.

Amplification of a chirped pulse in the XeF(C-A) amplifier was carried out with the use of the laser mixture containing 0.2 Torr XeF_2 and 0.5 bar nitrogen at $U_0 = 95$ kV. An output energy of 2.5 J was reached when a 2.4 ps seed pulse with an energy of about 1 mJ in a super-Gaussian beam was injected into the XeF(C-A) amplifier [51]. An autograph of the output laser beam on a photographic paper sheet is shown in **Figure 12**. The energy obtained in this experiment promises a peak power as high as ~50 TW to be attained in the visible after pulse recompression to the initial duration of 50 fs.

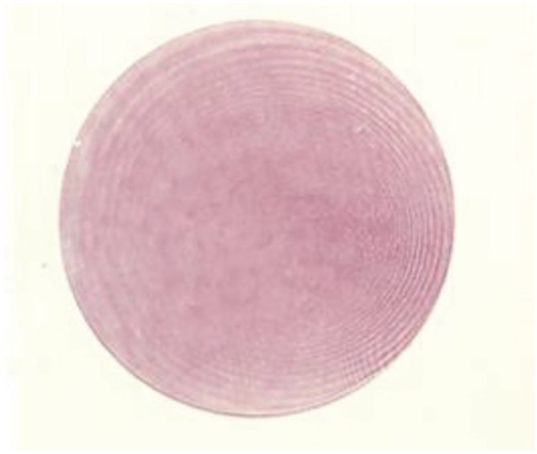

Figure 12. Imprint of the output laser beam with 2.5 J energy.

4. Wavelength scaling of laser-matter interaction

The visible spectrum of the hybrid femtosecond systems based on the XeF(C-A) amplifiers allows for the λ-scaling laser-matter interaction to be studied. Just to illustrate the role of laser-driver wavelength in laser-matter interaction we shall mention briefly some of applications in which the shorter laser wavelength provides advantages due to favorable wavelength scaling with special emphasis placed on the possible realization of a recombination soft X-ray laser operating in the "water window". The examples considered below do not cover all the applications in which the shorter laser wavelength may be favorable as compared with near IR solid-state femtosecond systems. Nevertheless, they show that the extension of laser wavelength to the visible region allows for wider experimental conditions to be realized providing different laser-matter interaction parameters and better understanding of the underlying physics.

4.1. Laser wake-field acceleration

Laser-driven plasma wake-field acceleration (LWFA) capable of producing high-energy electron beams is widely studied both theoretically and experimentally. In plasma-based acceleration, an intense laser beam drives large amplitude plasma waves via the ponderomotive force. The plasma wave can support very high longitudinal electric fields trapping and accelerating electrons. LWFA experiments have demonstrated acceleration gradients >100 GV m^{-1} enabling electrons to be accelerated well beyond GeV energy on a distance of about 1 cm using a 100 TW-class laser [55].

The electron energy gain ΔE is proportional to the acceleration length, L_{acc}, and longitudinal electric field, E_z, averaged over the acceleration length: $\Delta E = eE_zL_{acc}$. Among the factors limiting the effective acceleration length, laser diffraction, electron dephasing, and pump depletion are the most important. In experiments, the limiting role of the first factor is usually mitigated due to relativistic self-guiding or by using a preformed plasma channel. Electron dephasing originates from the difference of electron and plasma-wave propagation velocities. As a result, highly relativistic electrons, accelerated up to a velocity approaching the speed of light, outrun the accelerating phase region of the plasma wave propagating with a phase velocity, v_p, that is close to the laser pulse group velocity v_g and less than the electron velocity. Electrons are accelerated until their phase slips by one-half the plasma-wave period. In the most promising and efficient high-intensity limit corresponding to a nonlinear wake-field acceleration, referred to the blow-out, bubble, or cavitation regime, the radial ponderomotive force expels all the plasma electrons outward to create a electron density structure resembling a spherical ion cavity behind the laser pulse. Coulomb forces pull the electrons back to the axis in about a plasma period at the rear of the cavity to be trapped and accelerated by the wake-field until they reach the cavity center where they diphase. The acceleration length strongly depends on the plasma-wave phase velocity, which is close to the laser pulse group velocity, v_g, obeying the plasma dispersion low: $v_g = d\omega/dk \approx c(1-\omega_p^2/\omega_0^2)^{1/2}$ with ω_0 and ω_p being the laser and plasma frequencies, respectively. Due to the plasma dispersion, shorter wavelength laser pulses propagating with higher group velocity provide longer dephasing length, L_d. According to the estimations made in [51] with pump depletion taken into account, the dephasing length, given by $L_d \approx 4ca_0^{1/2}\ (\omega_0^2/3\omega_p^3)$ with $a_0 = eA/m_ec^2$ being the relativistically normalized laser amplitude, scales as ω_0^2 showing that shorter laser wavelengths are highly beneficial from the viewpoint of an increase in the acceleration length.

The detailed consideration [56] based on the phenomenological 3D theory for LWFA in the blowout regime, valid at laser power, P, exceeding the critical power $P_c = 17(\omega_0^2/\omega_p^2)$ [GW] for relativistic self-focusing, predicts the electron energy gain

$$\Delta E\left[\mathrm{GeV}\right] = 1.7\left(P\left[\mathrm{TW}\right]/100\right)^{1/3}\left(10^{18}/n_p\left[\mathrm{cm}^{-3}\right]\right)^{2/3}(0.8/\lambda_0[\mu\mathrm{m}])^{4/3}$$

where n_p is the plasma density, and λ_0 stands for the laser wavelength. This indicates that the λ-scaling of LWFA could be of great practical interest. Practically, the same λ-scaling has been

obtained in Ref. [57]. However, it should be noted that the gain in energy is achieved at the expense of reducing the number of accelerated electrons, which is proportional to the laser wavelength [56, 57].

4.2. High-order harmonic generation

High-order harmonic generation (HHG) is nowadays widely used to generate spatially and temporally coherent short-wavelength radiation when an intense optical field interacts with a gas or solid target. HHG can provide a single burst or train of attosecond pulses, which allow for ultrafast dynamics of electrons in atoms, molecules, or even solids to be explored [58]. (For a detailed review of experimental and theoretical developments in HHG, see, e.g., [58, 59].)

According to the generally accepted semiclassical three-step model of HHG in gases, the highest possible photon energy (cutoff energy, E_{cutoff}) in the high harmonic spectrum that can be generated from a single atom or ion is predicted by the universal law $E_{cutoff} = I_p + 3.17U_p$ [60]. Here, I_p is the ionization potential and $U_p = 9.33 \times 10^{-14} I_0 \lambda_0^2$ is the ponderomotive energy, which is the cycle-averaged kinetic energy of an electron in the laser electric field of intensity I_0 and wavelength λ_0. The λ_0^2 dependence of U_p implies that the use of long excitation wavelengths should result in extending the harmonic cutoff energy further into the X-ray region. On the other hand, conversion efficiency of HHG in gases strongly depends on laser wavelength. The λ-scaling at constant laser intensity has revealed the dependences of HHG efficiency to be between λ_0^{-5} and λ_0^{-6}, which have been obtained experimentally and from numerical simulations [61–63]. General scaling analysis of HHG efficiency as a function of drive laser parameters and material properties is given in [64], which predicts the scaling of the HHG efficiency with the driving wavelength to be λ_0^{-5} at the cutoff and λ_0^{-6} at the plateau region for fixed harmonic wavelength. The severe wavelength dependence of the HHG efficiency is associated with the single-atom dipole response and phase matching. Shorter driver wavelengths are advantageous for both of these factors, if the final objective is not to produce as high-energetic photons as possible. The experimental results obtained in Ref. [65] for different noble gases confirm this wavelength scaling and show two orders of magnitude higher HHG intensity in the energy range of 20–70 eV with 400 nm pulses as compared with 800 nm laser driver.

However, HHG in gases has fundamental physical restrictions arising from the limitation on the laser intensity since plasma generation, caused by strong ionization of the gaseous medium at intensities above 10^{16} W/cm^2, results in phase mismatch, thereby suppressing harmonic generation [66]. This limitation is not present in the case of HHG from solid. According to the oscillating plasma mirror model [67], the laser field produces a relativistic oscillation of the overcritical plasma surface with the laser frequency, inducing incident pulse modulation that gives rise to the high-order harmonics in the spectrum of the reflected emission due to a transient Doppler frequency upshift. (For more detailed analysis of the basic generation mechanisms lying behind HHG from solids, see, e.g., [59, 68, 69].)

Using particle-in-cell (PIC) simulation to accurately model the HHG with a plasma target, Teubner and Gibbon [59] have obtained the laser-to-harmonic conversion efficiency, η_H, in the laser intensity range $I_0 = 10^{17}$–10^{19} W/cm^2. Summarized by an empirical relation for high

harmonic orders ($N = \lambda_0/\lambda_H >> 1$, where λ_H stands for harmonic wavelength), the results of the numerical simulation take the form [54]:

$$\eta_H \approx 9'10^{-5}(I_0\lambda_0{}^2 / 10^{18}\,\mathrm{W\ cm^{-2}\mu m^2})^2 \left(N/10\right)^{-\alpha}$$

with α depending on the laser intensity and ranging from $\alpha = 6$ at $I_0 = 10^{17}$ W/cm^2 to $\alpha = 3.5$ at $I_0 = 10^{19}$ W/cm^2 at $\lambda_0 = 1$ μm. On the basis of this empirical scaling, the authors came to the conclusion that shorter wavelength lasers are highly beneficial from the viewpoints both of extending to shorter-wavelength harmonics and harmonic efficiency enhancement. The wavelength scaling of the same form but with $\alpha = 5$ independent of laser intensity was argued with the use of 1D-PIC code in the earlier paper of Gibbon [70]. The analysis made in [59] of a variety of experimental results obtained with different laser wavelengths confirms the prediction of the strong harmonic yield increase with laser frequency. This makes powerful blue-green hybrid systems to be very promising as the drivers for generation of soft X-ray harmonics well within the water-window spectral range.

4.3. Soft X-ray lasers

Development of coherent X-ray sources is motivated by a variety of their applications in science and technology. X-ray lasers offer new capabilities in understanding the nanoscale structure of complex materials, including biological systems, and X-ray matter under extreme conditions. One of the greatest challenges is the high-resolution 3D holographic microscopy of a wide range of biological objects in the living state. For this purpose, coherent ultrafast X-ray sources of high power are required. One of the most important milestones for the high contrast X-ray imaging of living biological structures in a natural aqueous environment is the "water window" lying between the K absorption edges of carbon (4.37 nm) and oxygen (2.33 nm), where carbon is highly opaque, while water is largely transparent. A primary challenge of X-ray exposure is the realization of "diffraction-before-destruction" approach allowing for diffraction patterns to be obtained on time scales shorter than the onset of radiation damage of samples. This approach has been successfully demonstrated in studies of biological samples with the use of X-ray free electron lasers (XFEL) producing femtosecond pulses of high intensity (For example, see [71]).

There has been remarkable progress in the development of XFELs that hold the great promise for user experiments ranging from atomic physics to biological structure determination. Despite the fact that these lasers are powerful tools in studies of matter structure and physics of light-matter interaction, they have limited accessibility because of their high cost and large-scale. This makes the current search for alternative X-ray sources of laboratory scale to be of great importance.

Presently, there are two main approaches to the development of compact ultrashort-pulsed sources of coherent soft X-ray: above considered HHG by gas and solid targets, as well as the generation of coherent X-ray radiation in the laser plasma. The first one is characterized by low-intensity soft X-ray radiation, insufficient for the realization of holographic imaging

methods. The laser plasma enables generation of lasing in the soft X-ray region with beam performances close to those of XFELs [72].

Actually, only collisional and recombination schemes of active media excitation to produce soft X-ray in a laser plasma are of practical interest. The first of them was realized in a laser plasma with high electron temperature, providing a population inversion on transitions between excited states of ions, which typically lie in the range 10–50 nm [72]. The most promising way to extend the spectral range of the X-ray lasers deeper into the X-ray region, including the "water window," lies in the further developing recombination scheme of excitation of transitions to the ground state of recombining fully stripped ions.

The first observation of the amplification on the transition to the ground state dates back to 1983 [73] when hydrogen-like lithium ions were excited in the laser plasma produced due to optical field ionization (OFI) by the UV radiation from a subpicosecond KrF laser. Later that year, this observation was confirmed in different experimental conditions [74–76]. The OFI approach to excitation of recombination soft X-ray lasers is particularly attractive since it produces fully stripped ions on a time scale of one period of the incident laser electric field and enables formation of cold electrons with low residual energy (for a linearly polarized laser pulse) providing favorable conditions for high-rate three-body recombination. Residual energy is proportional to the square of a pump laser wavelength and can be reduced by using a short-wavelength driver pulse.

An electron removed from an atom due to OFI interacts with the plane polarized laser field and acquires quiver energy of the coherent electron oscillation in the field and energy of electron drift along the laser field direction [77, 78]. For ultrashort pulses, the quiver energy is returned to the wave, and it does not contribute to residual energy. Most of the electrons are ionized within a narrow interval near the crest of the oscillating electric field because of the exponential dependence of the ionization rate on the electric field amplitude. Classically, the average drift energy, ε, of an electron depends on the phase mismatch, $\Delta\phi$, between the phase at which the electron is freed and the crest of the electromagnetic wave:

$$\varepsilon = 2\varepsilon_q \sin^2 \Delta\phi$$

where ε_q is the quiver energy ($\varepsilon_q = e^2E_0^2/4m_e\omega^2$ with E_0 and ω being the peak amplitude and angular frequency of the laser electric field $E = E_0 \sin\omega t$, respectively). Thus, the residual energy of electrons produced by OFI can be much lower than the electron quiver energy, and, secondly, shorter wavelength ionizing lasers are beneficial to achieve gain in the recombination scheme.

To demonstrate advantages of short-wavelength pumping, λ-scaling of the recombination excitation efficiency for the transitions to ground state was experimentally and numerically studied by different groups [76, 78, 79]. Numerical simulations of the small-signal gain on the $4s_{1/2}$–$3p_{3/2}$ transition at 23.2 nm in Ar^{7+} show that 400 nm pump laser radiation allows an increase in the small-signal gain on the $4s_{1/2}$–$3p_{3/2}$ transition at 23.2 nm in Ar^{7+} by more than an order of magnitude as compared with 800 nm pumping [80].

Simulation of the recombination gain formation on the 2 → 1 transition at 3.4 nm in H-like CVI pumped with a 400 nm pump laser has been performed in [81]. It was shown that the recombination gain as high as 180 cm^{-1} can be achieved on this transition using the driving pulse duration of 20 fs with peak intensity of 8×10^{18} W/cm^2 and 10 μm diameter focal spot. The key factor playing important role in the recombination mechanism of pumping is the non-Maxwellian nature of the distribution function after OFI [79, 81], which is strongly peaked near the zero electron energy. Ultrashort pumping time (<100 fs) is required to minimize heating and Maxwellization of electron energy distribution at the time scale of three-body recombination.

Less encouraging results have been obtained in Ref. [82], indicating that there are a number of issues, which have to be investigated experimentally for better understanding of the physical processes lying behind the optical production of recombination plasmas. This requires the development of ultrashort (20–50 fs) multiterawatt lasers in the UV or visible range as pumping sources.

5. Conclusions

Development of the photochemical method for exciting active media has resulted in the emerging of the new class of gas lasers in the spectral range extending from the NIR to UV regions. The most remarkable achievements of these studies belong to the visible range where no alternatives are available so far for the excitation of broadband gaseous active media (XeF(C-A), Xe_2Cl, and Kr_2F) that would not be strongly modified by transient absorption. This pave the way for the development of hybrid (solid/gas) laser systems towards petawatt peak power in the blue-green spectral region due to their broad amplification bandwidths, able to support as short as 10 fs pulses, and their relatively high saturation fluences (0.05–0.2 J cm^{-2}), promising as high as 10 TW peak power to be obtained from square cm of an output aperture.

To demonstrate the high potential of the hybrid approach relying on the optically driven broadband active media in the visible, two femtosecond hybrid systems are now under development with the aim of conducting proof-of-principle experiments: THL-30 at LPI, designed for about 5 TW of output peak power, and THL-100 at IHCE, designed to be ten times more powerful. Behind these systems is the amplification of the second harmonic of Ti:sapphire front ends in the power-boosting XeF(C-A) amplifiers driven by the e-beam-to-VUV flash converters. In the pilot experiments performed in the THL-100 system, peak power of 14 TW has been attained in the 50 fs pulse at the output energy of 0.7 J. After upgrading pumping source, an energy output has been enhanced up to 2.5 J in the 2.4 ps pulse before its recompression promising a peak power of 50 TW to be obtained. Besides spectral matching between a solid-state frond-end and gas XeF(C-A) amplifier, the nonlinear frequency upconversion results in efficient temporal cleaning of the ultrashort optical pulse, thereby providing a high contrast ratio for the output blue-green pulses produced by a hybrid laser chain. This was confirmed by the results of ASE measurements in the XeF(C-A) amplifier of the

THL-100 system, which argue that a contrast ratio of 10^{12}–10^{13} is feasible in the blue-green hybrid femtosecond systems with a peak power of about 100 TW.

By the example of LWFA, HHG, and recombination soft X-ray lasers, it was shown that, in some cases, application of shorter wavelength lasers (as compared to Ti:sapphire lasers operating in the NIR) for laser-matter interaction may be advantageous and extends the frontiers of experimental ability to provide deeper insight into the physical mechanisms of the laser-matter interaction. One of the greatest challenges is the development of recombination-pumped soft X-ray lasers that have potential to extend SXRL spectral range towards "water window" and beyond.

Actually, the above-discussed blue-green hybrid concept can be considered as an alternative to the direct nonlinear upconversion of intense NIR laser radiation to the visible with the use of second harmonic generation (SHG) technique. However, to the best of our knowledge, the highest peak power reached so far in the visible with SHG does not exceed 4 TW, producing the peak intensity in a focal spot diameter of about 3 μm as low as 3×10^{18} W/cm^2 because of poor beam quality [83]. Achieving higher parameters in Ti:sapphire laser systems with SHG meets serious technical problems arising from a variety of nonlinear effects in crystals at high intensities leading to a significant spatiotemporal degradation of beam quality [84]. Moreover, a broad spectrum of femtosecond pulses and strong nonlinear wave front distortion require application of very thin (0.5–1 mm) nonlinear crystals of large diameter (>10 cm). The technology of such crystals manufacture is not yet available. Nevertheless, a large ongoing effort is presently devoted to overcome these difficulties in SHG and to reach hundreds of TW at wavelength of the second harmonic [85, 86]. The hybrid (solid/gas) laser technology is free of these problems because peak powers of 0.1–1 TW are required for a seed pulse generated by the solid-state front end in order to extract most of the energy stored in the final gaseous amplifier.

At the same time, it is necessary to say that the hybrid systems relying on the photochemically driven boosting amplifiers are inferior to the all-solid-state systems from the view point of a pulse-repetition rate reaching 1 kHz at moderate output peak powers. The hybrid systems operating in the visible could be of interest for the use in low repetition rate experiments, which require an output peak power of tens and hundreds of TW. In the case of the Xe_2Cl active medium, repetition rates up to 10 Hz seems to be attainable with proper engineering.

Acknowledgements

The work was supported by the Russian Foundation for Basic Research (Grant No. 15-19-10021).

Author details

Leonid D. Mikheev[1,2*] and Valery F. Losev[3,4]

*Address all correspondence to: mikheev@sci.lebedev.ru

1 P.N. Lebedev Physical Institute, Russian Academy of Sciences, Moscow, Russia

2 National Research Nuclear University MEPhI (Moscow Engineering Physics Institute), Moscow, Russia

3 Institute of High Current Electronics, Siberian Branch, Russian Academy of Sciences, Tomsk, Russia

4 National Research Tomsk Polytechnic University, Tomsk, Russia

References

[1] Danson C, Hillier D, Hopps N, Neely D. Petawatt class lasers worldwide. High Power Laser Sci. Eng. 2015;3:e3. doi:10.1017/hpl.2014.52

[2] Bahk S-W, Rousseau P, Planchon TA, Chvykov V, Kalintchenko G, Maksimchuk A, Mourou GA, Yanovsky V. Characterization of focal field formed by a large numerical aperture paraboloidal mirror and generation of ultra-high intensity (10^{22} W/cm^2). Appl. Phys. B. 2005;80:823–832. doi:10.1007/s00340-005-1803-8

[3] Zuev VS, Mikheev LD. Photochemical Lasers. Chur: Harwood Acad. Publ; 1991. 103 p.

[4] Mikheev LD. Photochemical lasers on electronic molecular transitions. Quantum Electron. 2002;32:1122–1132. doi:10.1070/QE2002v032n12ABEH002355

[5] Mikheev LD, Tcheremiskine VI, Uteza OP, Sentis ML. Photochemical gas lasers and hybrid (solid/gas) blue-green femtosecond systems. Progr. Quantum Electron. 2012;36:98–142. doi:10.1016/j.pquantelec.2012.03.004

[6] Basov NG, Zuev VS. Short-Pulse Iodine Laser. Il Nuovo Cimento. 1976;31B:129–151.

[7] Brederlow G, Fill E, Witte KJ. The High-Power Iodine Laser. Berlin Heidelberg: Springer-Verlag GmbH; 1983. 183 p. doi:10.1007/978-3-540-39491-4

[8] Zuev VS, Ka1ulin VA. Scientific foundations of powerful photodissociation lasers (history of research in the 1960s at the Division of Quantum Radiophysics of the P N Lebedev Physics Institute). Quantum Electron. 1997;27:1073–1080. doi:10.1070/QE1997v027n12ABEH001112

[9] Zarubin PV. Academician Basov, high-power lasers and the antimissile defence problem. Quantum Electron. 2002;32:1048–1064. doi:10.1070/QE2002v032n12ABEH002348

[10] Brederlow G, Brodmann R, Eidmann K, Nippus M, Petsch R, Witkowski S, Volk R, Witte KJ. Performance of the Asterix III high power iodine laser. IEEE J. Quantum Electron. 1980;QE 16:122–125. doi:10.1109/JQE.1980.1070441

[11] Kirillov GA, Murugov VM, Punin VT, Shemyakin VI. High-power laser system Iskra-V. Laser Part. Beams. 1990;8:827–831. doi:10.1017/S0263034600009198

[12] Tittel FK, Marowsky G, Wilson WL, Smiling M. Electron beam pumped broad-band diatomic and triatomic excimer lasers. IEEE J. Quantum Electron. 1981;QE 17:2268–2281. doi:10.1109/JQE.1981.1070705

[13] Tang KY, Lorents DC, Huestis DL. Gain measurements on the triatomic excimer Xe_2Cl. Appl. Phys. Lett. 1980;36:347–349. doi:10.1063/1.91498

[14] Mikheev LD. Possibility of amplification of a femtosecond pulse up to the energy 1 kJ. Laser Part. Beams. 1992;10:473–478. doi:10.1017/S0263034600006716

[15] Hofmann T, Sharp T, Dane B, Wisoff P, Wilson W, Tittel F, Szabó G. Characterisation of an ultrahigh peak power XeF(C-A) excimer laser system. IEEE J. Quantum Electron. 1992;QE 28:1366–1375. doi:10.1109/3.135279

[16] Simon J. Ultrashort light pulses. Rev. Sci. Instrum. 1989;60:3597–3624. doi: 10.1063/1.1140516

[17] Tellinghuisen P, Tellinghuisen J, Coxon JA, Velazco JE, Setser DW. Spectroscopic studies of diatomic noble gas halides. IV. Vibrational and rotational constants for the X, B, and D states of XeF. J. Chem. Phys. 1978;68:5187–5198. doi:10.1063/1.435583

[18] Bibinov NK, Vinogradov IP, Mikheev LD, Stavrovskii DB. Determination of spectral dependence of the absolute quantum yield of XeF(B,C,D) excimer formation upon photolysis of XeF_2. Sov. J. Quantum Electron. 1981;11:1178–1181. doi:10.1070/QE1981v011n09ABEH008227

[19] Kono M, Shobatake K. Photodissociative excitation processes of XeF_2 in the vacuum ultraviolet region 105–180 nm. J. Chem. Phys. 1995;102:5966–5978. doi:10.1063/1.469331

[20] Mikheev LD, Stavrovskii DB, Zuev VS. Photodissociation XeF laser operating in the visible and UV regions. J. Rus. Las. Res. 1995;16:427–475. doi:10.1007/BF02581226

[21] Brashears HC, Setser DW. Transfer and quenching rate constants for XeF(B) and XeF(C) state in low vibrational levels. J. Chem. Phys. 1982;76:4932–4946. doi:10.1063/1.442839

[22] Basov NG, Zuev VS, Mikheev LD, Stavrovskii DB, Yalovoi VI. Stimulated emission due to the $B(1/2)$–$X^2\Sigma^+$ transition in the XeF molecule formed by photodissociation of XeF_2. Sov. J. Quantum Electron. 1977;7:1401. doi:10.1070/QE1977v007n11ABEH008201

[23] Basov NG, Zuev VS, Kanaev AV, Mikheev LD, Stavrovskii DB. Laser action due to the bound-free C(3/2)–A(3/2) transition in the XeF molecule formed by photodissociation of XeF_2. Sov. J. Quantum Electron. 1979;9:629. doi:10.1070/QE1979v009n05ABEH009058

[24] Zuev VS, Kashnikov GN, Mamaev SB. XeF laser with optical pumping by surface discharges. Quantum Electron. 1992;22:973–979. doi:10.1070/QE1992v022n11ABEH003645

[25] Knecht BA, Fraser RD, Wheeler DJ, Zietkiewich CJ, Mikheev LD, Zuev VS, Eden JG. Compact XeF (C → A) and iodine laser optically pumped by a surface discharge. Opt. Lett. 1995;20:1011–1913. doi:10.1364/OL.20.001011

[26] Knecht BA, Fraser RD, Wheeler DJ, Zietkiewich CJ, Mikheev LD, Zuev VS, Eden JG. Optical pumping of the XeF(C-A) and iodine 1.315-μm lasers by a compact surface discharge system. Opt. Eng. 2003;42:3612–3621. doi:10.1117/1.1751133

[27] Yu L, Liu J, Ma L, Yi A, Huang C, An X, Li H, Chen G. 10 J energy-level optically pumped XeF(C–A) laser with repetition mode. Optics Lett. 2007;32:1087–1089. doi:10.1364/OL.32.001087

[28] Gross RWF, Schneider LE, Amimoto ST. XeF laser pumped by high-power sliding discharges. Appl. Phys. Lett. 1988;53:2365–2367. doi:10.1063/1.100231

[29] Sentis ML, Tcheremiskine VI, Delaporte PC, Mikheev LD, Zuev VS. XeF(C-A) laser pumped by formed-ferrite open discharge radiation. Appl. Phys. Lett. 1997;70:1198–1200. doi:10.1063/1.118529

[30] Anisimov SV, Ermilov YuA, Kashnikov GN, Kazanskii VM, Mikheev LD, Nesterov RO, Stavrowskii DB, Theremiskine VI, Zemskov EM, Zuev VS. Spectrally selective time resolved actinometry of VUV radiation of a moving gas-dynamic discontinuity. Laser Phys. 1994;4:416–418.

[31] Eden JG. XeF(B → X) laser optically excited by incoherent Xe_2* (172-nm) radiation. Opt. Lett. 1978;3:94–96. doi:10.1364/ol.3.000094

[32] Bischel WK, Nakano HH, Eckstrom DJ, Hill RM, Huestis DL, Lorents DC. A new blue-green laser in XeF. Appl Phys. Lett. 1979;34:565–567. doi:10.1063/1.90868

[33] Eckstrom DJ, Walker HC, Jr. Multijoule performance of the photolytically pumped XeF (C-A) laser. IEEE J. Quantum Electron. 1982;QE 18:176–181. doi:10.1109/JQE.1982.1071517

[34] McCown AW, Eden JG. Ultraviolet photoassociative production of XeCl(*B*,*C*) molecules in Xe/Cl_2 gas mixtures: Radiative lifetime of $Xe_2Cl(4\ ^2\Gamma)$. J. Chem. Phys. 1984;81:2933–2938. doi:10.1063/1.448042

[35] Tittel FK, Wilson WL, Stickel RE, Marowsky G, Ernst WE. A triatomic Xe2Cl excimer laser in the visible. Appl. Phys. Lett. 1980;36:405–407. doi:10.1063/1.91533

[36] Basov NG, Zuev VS, Kanaev AV, Mikheev LD. Stimulated emission from an optically pumped Xe_2Cl laser. Sov. J. Quantum Electron. 1985;15:1289–1290. doi:10.1070/QE1985v015n09ABEH007742

[37] Zuev VS, Kanaev AV, Mikheev LD. Determination of the absolute quantum efficiency of the luminescence of Xe_2Cl^* in Cl_2–Xe mixtures. Sov. J. Quantum Electron. 1987;17:884–885. doi:10.1070/QE1987v017n07ABEH009473

[38] Mikheev LD. Evaluating the prospects of exciting the Xe_2Cl active medium by laser radiation for amplifying femtosecond pulses. Quantum Electron. 2005;35:984–986. doi:10.1070/QE2005v035n11ABEH013027

[39] Quiñones E, Yu YC, Setser DW, Lo G. Decay kinetics of XeCl(*B*,*C*) in Xe and in mixtures of Xe with Kr, Ar, Ne, and He. J. Chem. Phys. 1990;93:333–344. doi:10.1063/1.459605

[40] Okada F, Apkarian VA. Electronic relaxation of Xe_2Cl in gaseous and supercritical fluid xenon. J. Chem. Phys. 1991;94:133–144. doi:10.1063/1.460387

[41] Wiedeman L, Fajardo ME, Apkarian VA. Cooperative photoproduction of $Xe_2^+Cl^-$ in liquid Cl_2/Xe solutions: Stimulated emission and gain measurements. Chem. Phys. Lett. 1987;134:55–59. doi:10.1016/0009-2614(87)80013-1

[42] Zuev VS, Isaev IF, Kanaev AV, Mikheev LD, Stavrovskii DB, Shchepetov NG. Lasing as a result of a *B*–*X* transition in the excimer XeF formed as a result of photodissociation of KrF_2 in mixtures with Xe. Sov. J. Quantum Electron. 1981;11:221–222. doi: 10.1070/QE1981v011n02ABEH005884

[43] Zuev VS, Kanaev AV, Mikheev LD, Stavrovskii DB. Investigation of luminescence in the 420 nm range as a result of photolysis of KrF_2 in mixtures with Ar, Kr, and N_2. Sov. J. Quantum Electron. 1981;11:1330–1335. doi:10.1070/QE1981v011n10ABEH008468

[44] Basov NG, Zuev VS, Kanaev AV, Mikheev LD, Stavrovskii DB. Stimulated emission from the triatomic excimer Kr_2F subjected to optical pumping. Sov. J. Quantum Electron. 1980;10:1561–1562. doi:10.1070/QE1980v010n12ABEH010282

[45] Mikheev LD. Use of photoprocesses with charge transfer to excite active laser media. J. Sov. Las. Res. 1990;11:288–304. doi:10.1007/BF01120629

[46] Aristov AI, Grudtsin YaV, Zubarev IG, Ivanov NG, Konyashchenko AV, Krokhin ON, Losev VF, Mavritskii AO, Mamaev SB, Mesyats GA, Mikheev LD, Panchenko YuN, Rastvortseva AA, Ratakhin NA, Sentis M, Starodub AN, Tenyakov SYu, Uteza O, Tcheremiskine VI, Yalovoy VI. Hybrid femtosecond laser system based on photochemical XeF(C-A) amplifier with an aperture of 12 cm. Optica Atmosfery i Okeana J. 2009;22:1024–1029 (in Russian).

[47] Alekseev SV, Aristov AI, Grudtsyn YaV, Ivanov NG, Koval'chuk BM, Losev VF, Mamaev SB, Mesyats GA, Mikheev LD, Panchenko YuN, Polivin AV, Stepanov SG, Ratakhin NA, Yalovoi VI, Yastremskii AG. Visible-range hybrid femtosecond systems based on a XeF(C–A) amplifier: state of the art and prospects. Quantum Electron. 2013;43:190–200. doi:10.1070/QE2013v043n03ABEH015096.

[48] Hofmann T, Sharp TE, Dane CB, Wisoff P, Wilson WL, Jr, Tittel FK, Szabó G. Characterisation of an Ultrahigh Peak Power XeF(C-A) Excimer Laser System. IEEE J. Quantum Electron. 1992;QE 28:1366–1375. doi:10.1109/3.135279

[49] Sharp TE, Hofmann Th, Dane CB, Wilson WL, Tittel FK, Wisoff PJ, Szabó G. Ultrashort-laser-pulse amplification in a XeF(C-A) excimer amplifier. Opt. Lett. 1990;15:1461–1463. doi:10.1364/OL.15.001461

[50] Alekseev SV, Ivanov MV, Ivanov NG, Losev VF, Mesyats GA, Mikheev LD, Panchenko YN, Ratakhin NA. Modernization of THL-100 hybrid femtosecond laser system. Izvestiya Vysshikh Uchebnykh Zavedenii, Seriya Fizika. 2014;57(12/2):101–105 (in Russian).

[51] Alekseev SV, Ivanov MV, Ivanov NG, Losev VF, Mesyats GA, Panchenko YN, Ratakhin NA. Parameters of the THL-100 hybrid femtosecond laser system after modernization. Russ. Phys. J. 2015;58:1087–1092. doi:10.1007/s11182-015-0616-4

[52] Abdullin EN, Ivanov NG, Losev VF, Morozov AV. Production of a large cross-section electron beam in electron diode with rod reverse current conductors. Laser and Particle Beams. 2013;31:697–702. doi:10.1017/S026303461300075X

[53] Alekseev SV, Ivanov NG, Kovalchuk BM, Losev VF, Mesyats GA, Mikheev LD, Panchenko YN, Ratakhin NA., Yastremsky AG. Terawatt laser hybrid THL-100 system based on the photodissociation XeF(C-A) amplifier. Optica Atmosfery i Okeana J. 2012;25:221–225 (in Russian).

[54] Alekseev SV, Aristov AI, Ivanov NG, Kovalchuk BM, Losev VF, Mesyats GA, Mikheev LD, Panchenko YuN, Ratakhin NA. Multi-terawatt femtosecond hybrid system based on a photodissosiation XeF(C-A) amplifier in the visible range. Quantum Electron. 2012;42:377–378. doi:10.1070/QE2012v042n05ABEH014902

[55] Leemans WP, Gonsalves AJ, Mao H-S, Nakamura K, Benedetti C, Schroeder CB, Tóth CS, Daniels J, Mittelberger DE, Bulanov SS, Vay J-L, Geddes CGR, Esarey E. Multi-GeV Electron beams from capillary-discharge-guided subpetawatt laser pulses in the self-trapping regime. Phys. Rev. Lett. 2014;113:245002. doi:10.1103/PhysRevLett.113.245002

[56] Lu W, Tzoufras M, Joshi C, Tsung FS, Mori WB, Vieira J, Fonseca RA, Silva LO. Generating multi-GeV electron bunches using single stage laser wakefield acceleration in a 3D nonlinear regime. Phys. Rev. ST AB 2007;10:061301. doi:10.1103/PhysRevSTAB.10.061301

[57] Gordienko S, Pukhov A. Scalings for ultra relativistic laser plasmas and quasimonoenergetic electrons. Phys. Plasmas 2005;12:043109. doi:10.1063/1.1884126

[58] Eden JG. High-order harmonic generation and other intense optical field–matter interactions: review of recent experimental and theoretical advances. Prog. Quantum Electron. 2004;28:197–246. doi:10.1016/j.pquantelec.2004.06.002

[59] Teubner U, Gibbon P. High-order harmonics from laser-irradiated plasma surfaces. Rev. Mod. Phys. 2009;81:445–479. doi:10.1103/RevModPhys.81.445

[60] Krause JL, Schafer KJ, Kulander KC. High-order harmonic generation from atoms and ions in the high intensity regime. Phys. Rev. Lett. 1992;68:3535–3538. doi:10.1103/PhysRevLett.68.3535

[61] Yakovlev VS, Ivanov M, Krausz F. Enhanced phase-matching for generation of soft X-ray harmonics and attosecond pulses in atomic gases. Opt. Express 2007;15:15351–15364. doi:10.1364/OE.15.015351

[62] Tate J, Auguste T, Muller HG, Salières P, Agostini P, DiMauro LF. Scaling of wave-packet dynamics in an intense midinfrared field. Phys. Rev. Lett. 2007;98:013901. doi:10.1103/PhysRevLett.98.013901

[63] Colosimo P, Doumy G, Blaga CI, Wheeler J, Hauri C, Catoire F, Tate J, Chirla R, March AM, Paulus GG, Muller HG, Agostini P, DiMauro LF. Scaling strong-field interactions towards the classical limit. Nat. Phys. 2008;4:386–389. doi:10.1038/nphys914

[64] Falcão-Filho EL, Gkortsas VM, Gordon A, Kärtner FX. Analytic scaling analysis of high harmonic generation conversion efficiency. Opt. Express 2009;17:11217–11229. doi:10.1364/OE.17.011217

[65] Falcão-Filho EL, Lai C-J, Gkortsas V-M, Huang S-W, Chen L-J, Hong K-H, Kärtner FX. Scaling of high harmonic generation efficiencies with 400-nm and 800-nm driver pulses. In: Proceedings of Conference on Lasers and Electro-Optics and Quantum Electronics and Laser Science Conference (CLEO/QELS-2010); 16–21 May 2010; San Jose, California United States: IEEE; paper JThI4. doi:10.1364/CLEO.2010.JThI4

[66] Chen M-C, Arpin P, Popmintchev T, Gerrity M, Zhang B, Seaberg M, Popmintchev D, Murnane MM, Kapteyn HC. Bright, coherent, ultrafast soft X-ray harmonics spanning the water window from a tabletop light source. Phys. Rev. Lett. 2010;105:173901. doi:10.1103/PHYSREVLETT.105.173901

[67] Lichters R, Meyer-ter-Vehn J, Pukhov A. Short-pulse laser harmonics from oscillating plasma surfaces driven at relativistic intensity. Phys. Plasmas 1996;3:3425–3437. doi:10.1063/1.871619

[68] Thaury C, Quéré F. High-order harmonic and attosecond pulse generation on plasma mirrors: basic mechanisms. J. Phys. B: At. Mol. Opt. Phys. 2010;43:213001. doi:4075/43/21/213001

[69] Baeva T, Gordienko S, Pukhov A. Theory of high-order harmonic generation in relativistic laser interaction with overdense plasma. Phys. Rev. E. 2006;74:046404. doi:10.1103/PhysRevE.74.046404

[70] Gibbon P. Harmonic generation by femtosecond laser-solid interaction: a coherent "Water-Window" light source?. Phys. Rev. Lett. 1996;76:50–53. 10.1103/PhysRevLett.76.50

[71] Redecke L, et al. Natively inhibited *Trypanosoma brucei* cathepsin B structure determined by using an X-ray laser. Science. 2013;339:227–230. doi:10.1126/science.1229663

[72] Suckewer S, Jaeglé P. X-ray laser: past, present, and future. Laser Phys. Lett. 2009;6:411–436. doi:10.1002/lapl.200910023

[73] Nagata Y, Midorikawa K, Kubodera S, Obara M, Tashiro H, Toyoda K. Soft-x-ray amplification of the Lyman-alpha transition by optical-field-induced ionization. Phys. Rev. Lett. 1993;71:3774–3777. doi:10.1103/PhysRevLett.71.3774

[74] Nagata Y, Midorikawa K, Kubodera S, Obara M, Tashiro H, Toyoda K, Kato Y. Production of an extremely cold plasma by optical-field-induced ionization. Phys. Rev. A. 1995;51:1415–1419. doi:10.1103/PhysRevA.51.1415

[75] Korobkin DV, Nam CH, Suckewer S, Goltsov A. Demonstration of soft X-ray lasing to ground state in Li III. Phys. Rev. Lett. 1996;77:5206–5209. doi:10.1103/PhysRevLett.77.5206

[76] Goltsov A, Morozov A, Suckewer S, Elton R, Feldman U, Krushelnick K, Jones T, Moore C, Seely J, Sprangle P, Ting A, Zigler A. Is efficiency of gain generation in LiIII 13.5-nm laser with 0.25-μm subpicosecond pulses the same as with 1 μm?. IEEE J. Sel. Top. Quantum Electron. 1999;5:14531459. doi:10.1109/2944.814984

[77] Corkum PB, Burnett NH, Brunel F. Above-Threshold Ionization in the Long-Wavelength Limit. Phys. Rev. Lett. 1989;62:1259–1262. doi:10.1103/PhysRevLett.62.1259

[78] Penetrante BM, Bardsley JN. Residual energy in plasmas produced by intense subpicosecond lasers. Phys. Rev. A 1991;43:3100–3113. doi:10.1103/PhysRevA.43.3100

[79] Ditmire T. Simulations of heating and electron energy distributions in optical field ionized plasmas. Phys. Rev. E. 1996;54:6735–6740. doi:10.1103/PhysRevE.54.6735

[80] Spence DJ, Hooker SM. Simulations of recombination lasing in Ar^{7+} driven by optical field ionization in a capillary discharge waveguide. Opt. Commun. 2005;249:501–513. doi:10.1016/j.optcom.2005.01.031

[81] Avitzour Y, Suckewer S. Feasibility of achieving gain in transition to the ground state of C VI at 3.4 nm. J. Opt. Soc. Am. B 2007;24:819–828. doi:10.1364/JOSAB.24.000819

[82] Pert GJ. Scaling relations for the design of a recombination laser using tunneling ionization. J. Phys. B: At. Mol. Opt. Phys. 2009;42:225401. doi:10.1088/0953-4075/42/22/225401

[83] Toth R, Kieffer JC, Fourmaux S, Ozaki T, Krol A. In-line phase-contrast imaging with a laser-based hard x-ray source. Rev. Sci. Instrum. 2005;76:083701. doi:10.1063/1.1989407

[84] Begishev IA, Kalashnikov M, Karpov V, Nickles P, Schönnagel H. Limitation of second-harmonic generation of femtosecond Ti:sapphire laser pulses. J. Opt. Soc. Am. B. 2004;21:318–322. doi:10.1364/JOSAB.21.000318

[85] Mironov S, Lozhkarev V, Ginzburg V, Khazanov E. High-efficiency second-harmonic generation of superintense ultrashort laser pulses. Appl. Opt. 2009;48:2051–2057. doi: 10.1364/AO.48.002051

[86] Ginzburg VN, Lozhkarev VV, Mironov SYu, Potemkin AK, Khazanov EA. Influence of small-scale self-focusing on second harmonic generation in an intense laser field. Quantum Electron. 2010;40:503–508. doi:10.1070/QE2010v040n06ABEH014126

IntechOpen